Post-Print

This is the accepted version of:

P. Montinari, F. Gualdoni, A. Croce, C.L. Bottasso
Ultimate and Fatigue Load Mitigation by an Inertial-Driven Passive Flap, Using a Geometrically Exact Multibody Formulation
Journal of Wind Engineering and Industrial Aerodynamics, Vol. 175, 2018, p. 169-178
doi:10.1016/j.jweia.2018.01.038

The final publication is available at http://dx.doi.org/10.1016/j.jweia.2018.01.038

Access to the published version may require subscription.

Ultimate and fatigue load mitigation by an inertial-driven passive flap, using a geometrically exact multibody formulation

Pierluigi Montinari[b], Federico Gualdoni[b], Alessandro Croce[b], Carlo L. Bottasso[a,b,*]

[a] *Wind Energy Institute, Technische Universität München, D-85748 Garching b. München, Germany*
[b] *Department of Aerospace Science and Technology, Politecnico di Milano, 20156 Milano, Italy*

Abstract

The paper characterizes the performance of a passive flap concept when applied to a modern very large conceptual wind turbine. The passive flap responds automatically to blade and/or tower vibrations, inducing a change of camber that opposes dynamic loads on the wind turbine. This is obtained in a purely passive manner, without the need for actuators or sensors.

The present study is based on a detailed, geometrically exact multibody formulation of the device, which is able to capture all kinematic and structural dynamic effects of this inertia-driven device. The present modeling of the passive device improves on previous studies conducted with simplified models.

Results show a significant ability in the reduction of both fatigue and ultimate loads, including the case of flap-specific fault scenarios. Solutions for limiting losses in energy yield caused by non-null average flap rotations in the partial load region are also investigated. The present analysis motivates further studies aimed at reaping the benefits of load alleviation enabled by the passive flap, for example by designing a new enlarged rotor at similar key loads on the rest of the machine.

Keywords:
Wind turbine, Load mitigation, Passive flap, Aeroservoelasticity, Wind turbine control

Notation

c	Sectional chord
k	Stiffness
m	Mass
t	Time
C_H	Hinge moment coefficient
J	Moment of inertia
V	Wind speed

*Corresponding author, Tel.: +49 (0)89 289 16680.

α	Angle of attack
β	Blade pitch
δ	Flap deflection
τ	Gear ratio
Ω	Rotor angular speed
$(\cdot)^{NC}$	Non-circulatory term
$(\cdot)_{/*}$	Partial derivative, $\partial \cdot / \partial *$
$\dot{(\cdot)}$	Derivative wrt time, $\mathrm{d} \cdot / \mathrm{d}t$
ADC	Actuator duty cycle
AEP	Annual energy production
BEM	Blade element momentum
BTC	Bend twist coupling
CoE	Cost of energy
DEL	Damage equivalent load
DLC	Dynamic load case
EOG	Extreme operating gust
IPC	Individual pitch control
NTM	Normal turbulence model
NWP	Normal wind profile

1. Introduction and motivation

Wind energy has grown dramatically in the last fifteen years, to the point that it has become today the world principal source of renewable energy. Among many significant technological improvements that have enabled the success of wind energy, one aspect that clearly stands out is the continuous growth of the size of wind turbines. This growth trend is driven by at least two factors. Firstly, larger wind turbines capture more wind because of the greater area swept by their blades and because of their taller towers, leading to improved capacity factors. Second, all the rest being the same, installing and operating a smaller number of large machines implies significant advantages in logistics, grid connection, and operation & maintenance with respect to operating a larger number of small machines. This implies consequent benefits on the cost of energy (CoE). Clearly, optimal sizes for onshore and offshore applications may be very different, and also strongly depend on various local conditions.

In the future, the design of even bigger machines will most probably have to be enabled by suitable load mitigation technologies. In fact, the simple upscaling of existing solutions will not be economically and technically viable, due to the cubic law of growth: weight (and hence cost) grows cubically with size, implying an about ten-fold increase

when doubling the dimensions of a wind turbine. The present study falls within this general topic, and in particular it considers the assessment of the performance of a passive flap concept for the alleviation of ultimate and fatigue loads, when applied to a modern very large conceptual wind turbine.

The mitigation of loads can be obtained by different means. Full-blade span solutions involve the response of the entire blade. Individual pitch control (IPC) is a full-span active solution that has been studied extensively in the literature and that is now seeing an ever increasing acceptance by industry. Bend-twist coupling (BTC) is a full-span passive solution, which is not yet routinely adopted although it is being actively investigated (Bottasso et al., 2013; Bortolotti et al., 2017). However, although often very effective, any full-span solution is inherently somewhat limited in bandwidth, due to the inertia and non-local response of the blade.

On the other hand, distributed solutions locally affect the airloads by the use of pitchable tips/flaps/tabs (Andersen et al., 2010; Bergami and Poulsen, 2015; Bernhammer et al., 2016; Bottasso et al., 2016a,b; Chow and van Dam, 2007). The local nature of such solutions allows for a higher bandwidth in space and time, which may potentially result in an improved load mitigation effectiveness. In the case of actively controlled devices, the required moving parts, actuators and sensors will invariably increase the complexity of the rotor, which might in turn affect not only the cost of manufacturing, but also the cost of operation & maintenance and the availability of the machine, with possible consequent negative effects on the CoE. Therefore, deploying in the field a wind turbine with active distributed devices still posses some not fully solved challenges. As an alternative, passive devices –not requiring actuators and sensors– might be more appealing, if they can deliver significant load mitigation benefits at a greater simplicity.

An inertial-driven passive flap concept was proposed by Bottasso et al. (2016a) and Croce et al. (2016). The concept was further expanded to accommodate also the implementation by a passive tip in Bottasso et al. (2016b), albeit using a different physical phenomenon to drive the response of the device (see also Croce et al. (2016)). In the passive flap solution, the flap center of gravity is moved in front of the hinge line by the use of an offset mass. This way, flapwise accelerations of the blade excite a response of the flap that, by changing the airfoil camber, tend to oppose the acceleration itself, thereby attenuating dynamic blade loads. The flap is also aerodynamically balanced, in the sense that it is designed in order not to respond to the deliberate changes in angle of attack imposed by the wind turbine control system. Multiple load cases were considered in Bottasso et al. (2016a) through a loose coupling procedure between a state-of-the-art aeroservoelastic simulator and a typical section model. The preliminary analysis of that paper indicated a very promising performance of the novel device, which however had to be verified by a more sophisticated analysis.

It is the goal of the present paper to perform a complete aeroservoelastic analysis of the system, using a detailed multibody model of a wind turbine equipped with passive flaps. The multibody formulation is based on an exact fully nonlinear formulation of the geometry, kinematic and dynamics of the system, based on three dimensional rotation theory. The only linear assumption is in the beam model, which assumes a linear proportionality of internal stress resultants on sectional strains through a possibly fully populated stiffness matrix, something that is perfectly valid in the present context. However, all effects due the three dimensional relative motion of the system rigid and flexible bodies

and their connecting mechanical joints is rendered exactly. The mathematical model is hence capable of capturing the exact structural dynamics of the system without approximations, except for vanishingly small numerical effects. This is particularly important in the case of the passive flap, because the inertial forces that drive its motion (including gravity, which acts as a disturbance) depend in a complicated manner on the exact geometry of the system, including its deformation. The model is coupled with an unsteady aerodynamic model of the flap, together with a blade-element momentum (BEM) model of the rotor wake. The passive flap concept is applied to the conceptual INNWIND.EU 10 MW wind turbine (INNWIND.EU, 2017).

A second objective of the paper is the study of the possible impact of the proposed passive flap on the power capture of the rotor. In fact, non-null average flap rotations may reduce the rotor efficiency. If this happens in the partial load region, then energy yield may be affected. Two solutions are investigated: a simple constant preload, and a more sophisticated rotor-speed-varying preload implemented through a screw joint, inspired by the work of Bottasso et al. (2016b). In fact, differently from what was found in Bottasso et al. (2016a), the more sophisticated mathematical model used in the present investigation showed that the inertial coupling effects induced by precone/prebend of the blade and up-tilt of the rotor axis make it difficult to obtain small flap rotations without restraining it at the hinge. A detailed explanation of the phenomenon is provided in section 2. Results obtained in the present study indicate that modest average flap rotations, and hence modest losses in annual energy production (AEP), can be achieved by the simplest of the two solutions.

There are few alternatives to the passive flap concept presented in the literature. A different passive device is described by Lambie et al. (2011), where a passive camber control concept is investigated using a 2D aeroelastic typical section. A variation of airfoil camber is obtained by exploiting the chordwise aerodynamic load distribution, which changes as a function of angle of attack, while the original shape is restored by the use of a spring/damper system. A significant decrease of load fluctuations is shown by simplified load cases. However, this device will not only respond to undesirable changes of angle of attack due to blade vibrations, but also to the deliberate changes caused by the full-span pitching of the active control system that is responsible for the normal and emergency operation of the machine. In addition, the flexible airfoil camber will also change with the operating condition. This might impact the energy yield in the partial load regime, where the rotor should operate at maximum efficiency. A more recent analysis is reported in Marten et al. (2015), where a nonlinear lifting line free vortex wake model is employed to assess the performance of the passive device on a multi-megawatt wind turbine. Results indicate a reduction of the standard deviation of blade root bending moments, although a single simulation was considered and the energy yield was not analyzed.

The present paper is organized according to the following plan. At first, the working principle of the passive flap concept is reviewed, together with the structural dynamics and aerodynamic models used for the simulation of the wind turbine equipped with the flap. The sizing of the device is discussed next. Turbulent wind simulations are performed with the goal of identifying an optimal choice of flap parameters. To limit the effects of non-null average

flap rotations on rotor efficiency, which may impact energy yield, the two solutions of constant and rotor-speed-varying preload are investigated. After having sized the device, a more complete assessment of its overall performance is studied, including its effects on AEP, fatigue and ultimate loads at a few critical verification points on the wind turbine. All results are compared to those obtained on the same machine without the passive flap, indicating interesting load mitigation capabilities at modest AEP losses. The analysis is completed by the definition and study of a flap-specific fault scenario. Results indicate that faults do not change the design-driving loads, and therefore do not alter the load reducing capabilities of the passive device. Finally, conclusions and an outlook on further developments are given in the closing section of the paper.

2. Flap concept, models and methods

Figure 1 shows a wind turbine equipped with one passive flap per blade.

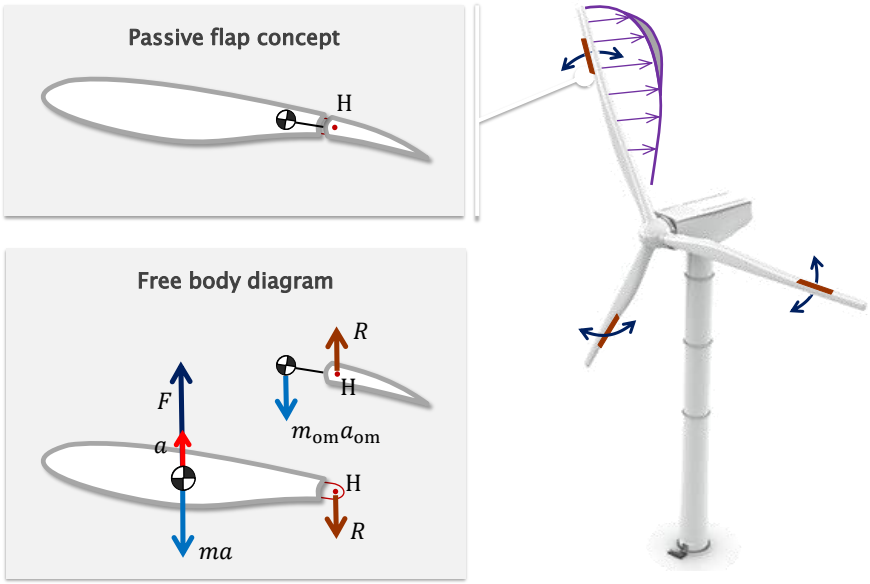

Figure 1: Wind turbine equipped with passive flaps, and explanation of the self-actuation mechanism by a free body diagram.

The passive device moves in response to out-of-plane accelerations, which occur when the blade flaps and/or the tower swings fore-aft. The flap response is driven by the inertia of an offset mass. As shown in the top left box of Fig. 1, an offset mass is installed in front of the hinge line H, and moves in the existing void between the pressure and suction sides of the blade, behind the aft shear web. The bottom left box of the same figure explains the self-actuation mechanism of the passive flap by means of a free body diagram, considering for simplicity only the effects on the offset

mass m_{om}. When the blade is –for example– pushed vertically up in the figure by force F, it accelerates in the same direction, and its vertical equilibrium according to D'Alembert is given by the balance among F, the force reaction R at the hinge H and the inertial force ma. Considering now the flap as a free body, due to the presence of the reaction force R at the hinge, an inertial force $m_{om}a_{om}$ is generated at the offset mass. In turn, thanks to its non-null arm with respect to the hinge line, such inertial force generates a moment that deflects the flap. In the example, the flap will rotate trailing edge up: this results in a reduction of the airfoil camber that tends to opposes the originating driving force F. Clearly, the flap will rotate trailing edge down when the blade is driven in the opposite direction, i.e. vertically down in the example of the figure. This passive mechanism results in the suppression of vibrations and dynamic loads, with a consequent reduction in fatigue and ultimate loads on the machine (Bottasso et al., 2016a).

The parameters of the passive flap need to be properly tuned, in order to deliver the best possible performance while satisfying the following requirements:

1. The flap spanwise extent and location should create a sufficient load authority, without affecting energy yield. This means that the flap should not significantly decrease the overall aerodynamic efficiency of the rotor in the partial load region (or region II, between cut-in and rated wind speed).
2. Flap chord, hinge line, offset mass and position should be such that the balancing mass can move freely within the aft part of the blade section, without interfering with suction and pressure-side skin panels and aft web.
3. The passive flap should not respond to deliberate blade pitch angle variations generated by the on-board control system, thus avoiding interfering with the control system goals of wind speed regulation, load alleviation, damping enhancement and shutdown handling. A way to fulfill this requirement is to design the flap with a certain degree of aerodynamic balancing, i.e. with a limited sensitivity of the aerodynamic hinge moment with respect to changes in angle of attack of the blade section (Bottasso et al., 2016a,b).

The first requirement is strictly related to the regulation strategy of a wind turbine. To optimize power capture in the partial load region, the rotor is governed so as to operate at its point of maximum efficiency (Bottasso et al., 2011). Since a passive flap modifies the airfoil camber, a non-zero mean flap rotation would invariably result in a loss of AEP, an effect that should clearly be avoided. This problem can be alleviated by using a hinge preload to keep the flap on average around its nominal position. Since thrust and torque, and hence loads in general, change throughout the partial load region, the preload can be scheduled with respect to the operating condition for a better average alignment of the flap. On the other hand, in the full power regime (or region III, between the rated and cut-out wind speeds) there is an excess of power in the wind, and the regulation strategy is to limit power output to its nominal rated value. In this case, a change in the efficiency of the blade is not an issue, and the wind turbine controller will automatically compensate for the flap misalignment by adjusting the blade pitch setting accordingly.

To more precisely illustrate the characteristics of the passive flap, a simple spring mass system can be used, following Bottasso et al. (2016a). The present study will however use a more sophisticated multibody model of the flapped wind turbine for a more realistic evaluation of the overall device performance, as illustrated later on in this work. The

linearized one degree of freedom flap model can be written as

$$J_\delta \ddot{\delta} + K_\delta \delta = M_a + M_p + M_i, \tag{1}$$

where δ is the flap rotation (positive for trailing edge toward-pressure-side displacements), J_δ the flap inertia including the presence of the offset mass, K_δ the hinge stiffness, M_a the aerodynamic moment, M_p the hinge preload and M_i a moment induced by inertial coupling effects. This last term is caused by the offset mass and it can be written as the sum of a moment M_Ω due to rotor speed and a moment M_g due to gravity, i.e.

$$M_i = M_\Omega + M_g. \tag{2}$$

Both terms are related to the precone and/or prebend of the blade, and to the up-tilt angle of the rotor shaft. In fact, when precone and/or prebend are different from zero, the centrifugal force acting on the offset mass has a component about the hinge line that generates a moment (constant with respect to the azimuthal blade position). In addition, a cyclic hinge moment at the 1P harmonic frequency is caused by gravity. It should be noted that the same mechanisms will generate also disturbing moments whenever the blade flaps out of plane. Furthermore, due to the shaft up-tilt, the out-of-plane weight component will generate an additional constant moment about the flap hinge. Smaller effects will be caused by the pitching and twisting of the blade, and more in general by the deformation of the whole wind turbine system. The complexity of these kinematic and dynamic couplings motivates the use of a geometrically exact multibody formulation to account for all effects without approximations.

The aerodynamic moment M_a can be expressed as follows:

$$M_a = q S_f c_f C_H + M_a^{NC}, \tag{3}$$

where q is the dynamic pressure, S_f the flap surface, c_f the flap chord and C_H the hinge moment coefficient, which takes the form

$$C_H = C_{H0} + C_{H,\alpha}\alpha + C_{H,\delta}\delta, \tag{4}$$

where M_a^{NC} is the non-circulatory unsteady correction term (Theodorsen, 1942; Bottasso et al., 2016a). When the flap is aerodynamically balanced (ESDU AERO C.04.01.03, 1989), the sensitivity of the hinge moment coefficient to changes in the angle of attack α, noted $C_{H,\alpha}$, becomes negligible for high thickness/chord ratios compared to the sensitivity with respect to flap deflections $C_{H,\delta}$. Values used in this work were extrapolated from the ESDU database, using a flap chord equal to 25% of the blade local chord and an overhang (defined as the non-dimensional distance between flap leading edge and hinge line) equal to 53% of the flap chord.

The hinge preload M_p can be used to keep the mean flap deflection around zero. A constant preload can be achieved with a spring, whose tuning is based on a compromise between load mitigation and AEP loss. However, since both inertial and aerodynamic loads are functions of the operating condition, a better mean flap alignment can be obtained by a varying preload. Scheduling the preload with the wind speed would require a wind speed estimator. A scheduling

with the rotor speed is possibly a simpler and more reliable solution, since it can be realized mechanically by the use of a screw joint, as shown by Stroub (1982) and Bottasso et al. (2016b). The limit of such a solution is that the preload is constant whenever rotor speed is constant. While this is not a problem in the full load regime, as previously mentioned, this would result in a constant preload in machines that present a transition regime (region II$^1/_2$) between the partial and full load conditions.

With a screw joint, the centripetal acceleration of the passive flap mass can be used to generate a rotor-speed-varying preload. In fact, as a consequence of the flap deflection δ, the screw generates a linear displacement z parallel to the hinge axis. This way, the preload becomes $M_p = \tau(F_c + F_g) + M_0$ and Eq. (1) modifies to the following expression

$$\bar{J}_\delta \ddot{\delta} + K_\delta \delta = M_a + M_i + \tau(F_c + F_g) + M_0, \tag{5}$$

where $\tau = z/\delta$ is the transmission ratio of the joint, M_0 the constant preload value and F_c and F_g the centrifugal and gravitational forces on the offset mass, respectively. The combined moment of inertia is expressed as:

$$\bar{J}_\delta = J_\delta + \tau^2 m, \tag{6}$$

where m is the total flap mass. The centrifugal force can be approximately expressed as

$$F_c = m(r+z)\Omega^2, \tag{7}$$

where r is the distance of the flap mass to the rotor axis. Inserting Eq. (7) into Eq. (5), one gets:

$$\bar{J}_\delta \ddot{\delta} + (K_\delta - \tau^2 m\Omega^2)\delta = M_a + M_i + \tau m r\Omega^2 + \tau F_g + M_0, \tag{8}$$

which shows that the effective stiffness of the system decreases by $\tau^2 m\Omega^2$. The gravitational force is expressed by:

$$F_g = mg\cos\psi, \tag{9}$$

where ψ is the blade azimuthal position and g the acceleration of gravity. The transmission ratio τ and the constant M_0 are chosen to balance the mean of the right hand side of Eq. (8), i.e.:

$$\tau m r\Omega^2 + M_0 = -(M_a + M_i). \tag{10}$$

The term F_g is not considered in Eq. (10), since it is a periodic disturbance with zero mean. Notice once again that the previous simplified model is only used for an explanation of the concept of the rotor-speed-varying preload and its preliminary sizing. However, all simulations performed in the present study are based on the geometrically exact multibody formulation described in §2.1.

Figure 2 shows the mean flap deflections obtained with the rotor-speed-varying preload compared with the solution with a constant preload. Results refer to normal wind profile (NWP) simulations performed over the entire operating range of the machine. The plot highlights that, with the rotor-speed-varying preload, the flap misalignment is limited between 0 and 5 deg from 7 to 11 m/s (region II). In the same speed range, the solution with a constant preload has a much larger flap excursion, between 17 and -7 deg. Large flap rotations are present in both cases in the full power range, which is however not a problem because they will be automatically compensated for by the pitch control system.

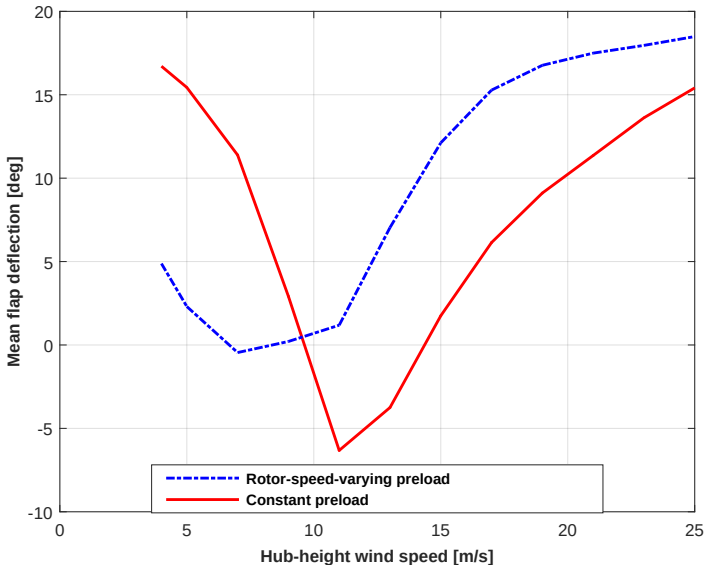

Figure 2: Mean flap misalignment over the wind turbine operating range. Comparison between a passive flap with constant (red solid line) and rotor-speed-varying preload (blue dash-dotted line).

2.1. Geometrically exact aeroservoelastic multibody model

The present study investigates the application of the passive flap concept to the INNWIND.EU 10 MW wind turbine (INNWIND.EU, 2017; Bak et al., 2013), which is a conceptual model of a modern very large offshore machine.

The simulation model is based on a multibody formulation, implemented in the aeroservoelastic code `Cp-Lambda` (Code for Performance, Loads, Aeroelasticity by Multi-Body Dynamic Analysis) (Bauchau et al., 2001b, 2003; Bottasso and Croce, 2006–2017). A topological view of the model is shown in Fig. 3, and it is realized by nonlinear flexible beam elements, rigid bodies, joints, actuators, sensors and aerodynamic models. The multibody index-3 formulation is expressed in terms of Cartesian coordinates (Bottasso, 2010), while constraints are enforced by scaled Lagrange multipliers (Bauchau et al., 2009). Joint models optionally include internal springs and dampers, friction, contact and freeplay (Bauchau et al., 2001a). Rotor blades, flaps and tower are described by nonlinear geometrically exact shear and torsion deformable beam models, including off-diagonal stiffness couplings. Flexible components are discretized in space by the finite element method, leading to a system of differential algebraic equations in the time domain. Time integration is performed by a non-linearly unconditionally stable scheme that includes high frequency dissipation by energy decay (Bauchau et al., 2003). Sensors can be used to output quantities of interest at arbitrary points in the model, and they are also used to implement user-defined control laws through a standard user interface.

The aerodynamic behavior of the blade is modeled by a lifting line, which accounts for the spanwise chord and twist distributions and the sectional characteristics of the airfoils. Lift, drag and moment aerodynamic coefficients are evaluated by the open-source software `XFoil` (Drela et al., 2001) and stored in look-up-tables scheduled in terms of angle of attack, flap deflection and Reynolds number. The flap aerodynamics is modeled using thin airfoil theory. The

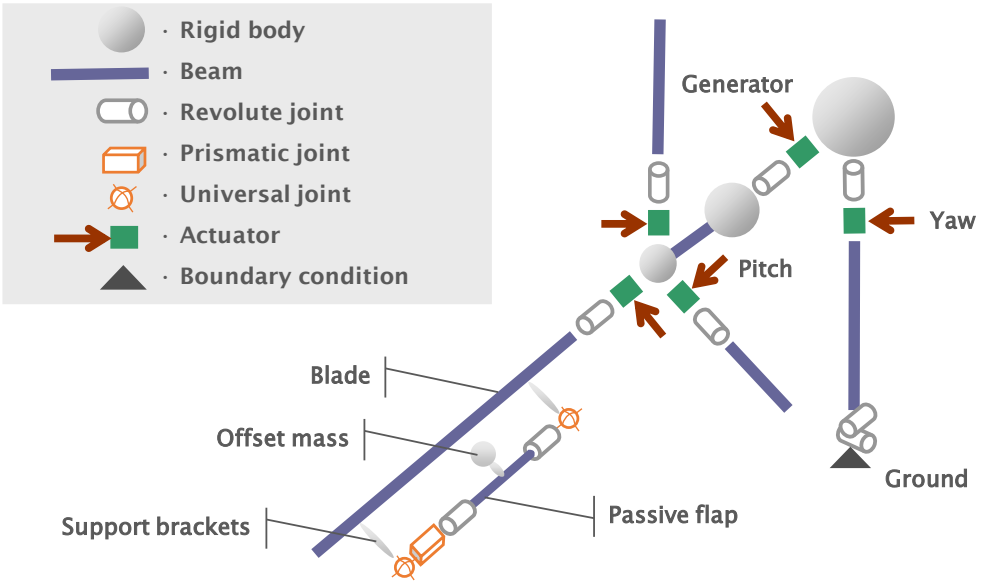

Figure 3: Topological sketch of the wind turbine model equipped with passive flaps. One single flapped blade is shown, for clarity.

steady sectional hinge aerodynamic derivatives are estimated with the ESDU semi-empirical method (ESDU 89010, 1989) and parameterized as functions of angle of attack and flap deflection. Post-stall corrections due to control surface deflection are computed according to the WSU model (Wentz et al., 1980). Non-circulatory coefficients are included according to the theory of Theodorsen (Theodorsen, 1942; Bottasso et al., 2016a). Unsteady circulatory effects are accounted for by the state space formulation of the 3D inflow model based on the unsteady flow theory over a circular disk with a pressure jump (Peters and Cheng, 1995).

The overall structural flap assembly is implemented by a multibody representation of a possible actual mechanical implementation of this device (Bauchau et al., 2001b,a), as shown in Fig. 3. The flap itself is modeled by a geometrically exact beam, connected to another beam modeling the blade. To accommodate the respective deformations of blade and flap, the attachment of the flap to the blade is realized avoiding hyperstatic constraints. The flap hinges are represented by revolute joints with internal springs, which are chosen so as to place the flap natural frequency of vibration at a desired value. The hinges are in turn connected to the supporting brackets on the blade by universal joints, which free the rotations of the flap tips. In addition, a prismatic joint at the outboard bracket frees the axial degree of freedom, which prevents the axial loading of the flap when the blade bends in-plane or twists. Finally, rigid bodies are used to model the offset masses in front of the hinge line. Since the model is based on a geometrically exact formulation, all static, kinematic and dynamic effects and couplings are rendered without approximations.

The effects of the wake are modelled by a classical BEM theory based on annular stream tube with wake swirl and unsteady correction (Hansen, 2008). The aerodynamic description is completed by root and blade tip losses, dynamic

stall, 3D blade root delayed stall and rotor-tower interference models. Deterministic effects, such as wind shear and tower shadow, are also included as specified by IEC 61400-1 (2005). The wind field includes deterministic gusts and turbulent time histories, the latter obtained by the open-source software `TurbSim` (Kelley and Jonkman, 2015).

The machine is governed over its entire operating range by controllers interfaced with the wind turbine model by external dynamic libraries. A supervisory controller manages the machine behavior by switching among the different operating states, and also handles emergencies. The model is completed by a collective-pitch/torque controller, based here on the implementation described in Bak et al. (2013).

3. Passive flap sizing

Tuning of the passive flap parameters aims at maximizing the load mitigating effects of the device and minimizing AEP losses, while respecting the design criteria exposed earlier on. The offset mass and distance in front of the hinge line determine the flap deflection response characteristics, with consequent direct effects on loads and performance. The sizing of these two quantities is performed by a partial fatigue assessment, obtained by parametric aeroservoelastic simulations in normal turbulence model (NTM) at wind speeds of 9, 11 and 13 m/s, where fatigue loading is higher. After sizing, a more complete load assessment of the two most interesting flap configurations is performed in the next section.

The flap occupies 25% of the sectional chord, while two different spanwise apertures are considered, between 70% and 80% span and between 70% and 85% span, the second providing for an increased load authority of the device. The overhang is chosen to aerodynamically balance the flap, i.e. to obtain a negligible hinge moment rate of change with respect to the angle of attack. The flap deflection stiffness, provided by the hinge-internal springs, is selected to achieve a flap natural frequency significantly below the 1P, which was shown to be an effective choice in Bottasso et al. (2016a).

Figure 4 reports changes in the Weibull-weighted damage equivalent load (DEL) combined bending moment at blade root, as functions of these two parameters. The x axis of the plot shows the mass offset distance in front of the hinge line, expressed in terms of percentage of the average chord length in the flapped portion of the blade. For values above about 22% of the offset distance, the plot is shaded in grey to indicate that the mass would interfere with the aft web. The y axis of the plot shows the offset mass, expressed as a percentage of the blade sectional mass per unit length. Isolines are labelled by DEL changes with respect to the baseline wind turbine without flaps, negative numbers indicating a reduction in fatigue loading.

Although DEL reductions for this load are small, a minimum is present for a mass of 18% in the non-shaded portion of the plot. Given that the flap occupies 10% of the blade span, the total offset mass is 0.75% of the blade mass. Considering the presence of the web constraint, a reasonable choice for the offset is about 21%. These two values of mass and distance are used in the remainder of this work. The shape of the plot is readily explained considering that the combined DEL is obtained by both flapwise and edgewise contributions. The former component of fatigue loading

in general benefits from larger masses placed farther in front of the hinge line, because this gives a greater effectiveness to the passive flap in opposing blade dynamic loads. On the other hand, edgewise loading is mostly due to gravity, while aerodynamically induced edgewise loads play a lesser role. Therefore, edgewise DELs, while being essentially insensitive to the offset distance, increase for larger offset masses, since these create additional significant 1P harmonic loading with their large moment arm with respect to the blade root. The combination of these two different behaviors of the flapwise and edgewise DELs results in the isolines shown Fig. 4.

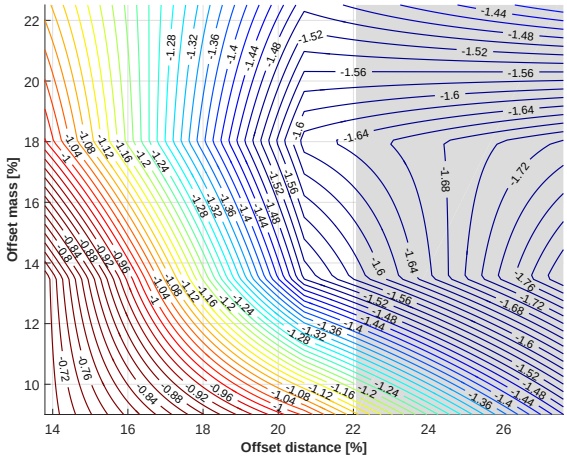

Figure 4: Weibull-weighted DEL combined bending moment at blade root, as function of offset mass and distance in front of the hinge line. Isolines are labelled by changes with respect to the baseline wind turbine without flaps, negative numbers indicating a reduction in fatigue loading.

Larger DEL reductions are obtained in the fixed system. Figure 5 at left shows DEL variations for the combined hub moment, which is mostly due to blade flapping. The same figure at right gives the combined bending moment at tower base, whose prevalent orientation is in the fore-aft direction, mostly caused by thrust fluctuations. For the offset mass and distance that realize a minimum for blade root DELs, fatigue at the hub is reduced by 3.5% and at tower root by 12%.

The addition of the offset mass in the flap alters the natural frequencies of the machine. A simplified Campbell diagram, shown in Fig. 6, is used to verify the absence of resonant phenomena and the correct placement of all natural frequencies. The plot does not report the rotor whirling modes, not to clutter the picture. Only minor differences are found for the first two fore-aft and side-side tower modes. The three lowest out-of-plane rotor modes (the first two being asymmetric, the third symmetric) appear to be lowered by around 2%. However this is still acceptable, since crossing of the 3P is at approximately 120% of the rated rotor speed. Finally, the lowest two rotor in-plane modes are reduced by around 3%, which again does not create any resonance issues. The passive flap mode is at a very low frequency of 0.014 Hz, and therefore it does not appear in the figure.

The hinge preload plays an important role in the tuning of the passive flap, since it determines the mean flap deflection, which impacts the rotor aerodynamic efficiency. To quantify this effect together with fatigue mitigation,

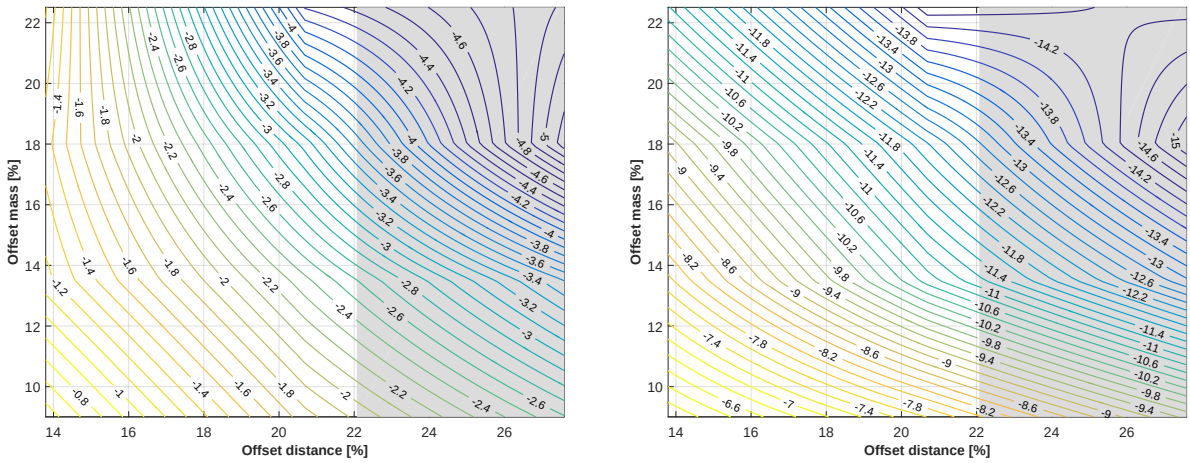

Figure 5: Variations in Weibull-weighted combined DELs at hub (left) and tower base (right).

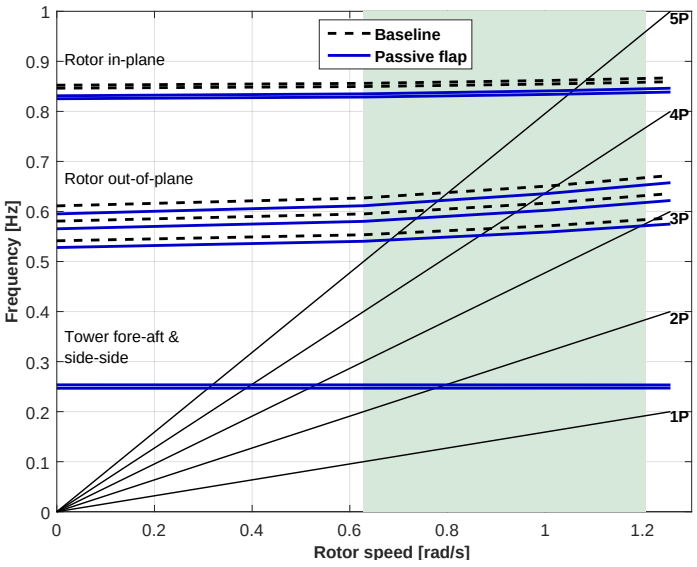

Figure 6: Simplified Campbell diagram with and without passive flap. The shaded green area represents the operating range from cut-in to 120% rated rotor speed.

NTM simulations are conducted over the entire operating range of the machine. Two solutions are considered: the rotor-speed-varying preload obtained by the use of a screw joint, and the simpler constant preload. In the latter case, three different values of the preload are analyzed, which realize null flap rotations at wind speeds of 7.5, 9.5 and 10.5 m/s, the first value being also the Weibull most probable speed for a Class IA wind turbine.

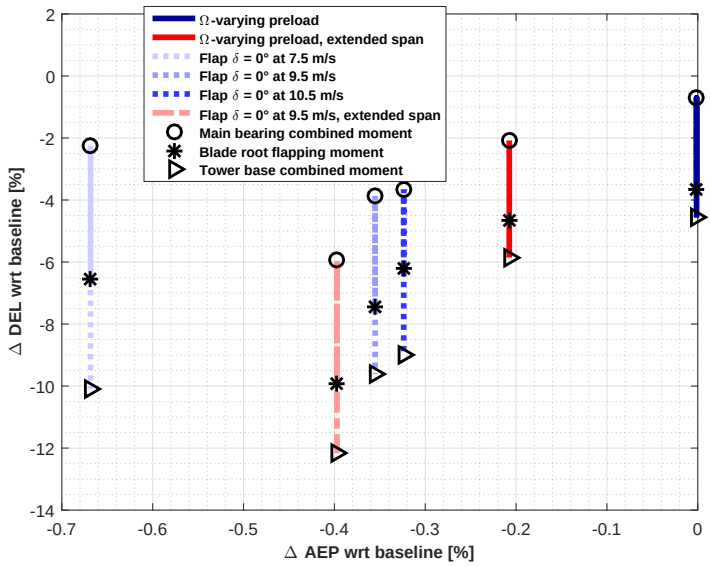

Figure 7: DEL vs. AEP percent variations.

Results are shown in Fig. 7, which shows DEL reductions as functions of AEP variations in percent values. Each solution is represented as a vertical bar reporting, at a certain AEP value, the corresponding DELs measured for the blade root flap component (indicated by an asterisk), hub combined moment (indicated by a circle) and tower base combined moment (indicated by a right facing triangle).

The dark blue solid bar on the right side of the graph refers to the case with rotor-speed-varying preload. As expected, AEP losses are very small (essentially null) because of the small average misalignment of the flap throughout the partial load region. On the other hand, DEL reductions are limited, and go from around 1% on the main bearing to about 4.5% at tower base. The reduced effectiveness of the device is due to the scheduling mechanism. In fact, the preload is generated by the forces acting on the flap mass through the transmission ratio τ (cf. Eq. (5)), with disturbances introduced by gravity, blade deformation and pitching, as well as flap deflection. In particular, gravity cyclically pulls on the flap, creating a radial displacement that, through the screw joint, induces a flap rotation, which in turn creates a 1P airload component that causes an increment of DEL.

The three blue dashed bars correspond to the constant preload cases. The AEP decreases when the preload is tuned for lower values of the wind speed. An interesting solution appears to be the one when preload is tuned for 9.5 m/s, since its has a rather limited loss in AEP of 0.33%, with good overall DEL reductions. A more complete analysis would

be necessary to identify the best trade-off. In general load reductions are best exploited in terms of CoE by designing larger rotors at similar key loads, as shown for example by Bortolotti et al. (2017).

The red bars present the results obtained by a 50% increase of the flapped portion of the blade, which now occupies the position from 70% to 85% span. The flap parameters, including offset percent of sectional mass and distance, are the same as in the previous cases. The solid bar represents the case with rotor-speed-varying preload; AEP losses are a bit increased with respect to the smaller flap extension, but still small. On the other hand, DELs are further reduced, and go from around 2% on the main bearing to about 6% at tower base. The dash-dotted bar represents the case with constant preload tuned to achieve a null flap rotation at 9.5 m/s. As expected, results show an increased load reduction capability, due to the augmented authority of the device, but at the expanse of a further loss of AEP.

Table 1 summarizes the main flap parameters that will be used for the more detailed analysis on fatigue and ultimate loads presented in the next section.

Table 1: Main parameters of the passive flap for the 10 MW wind turbine.

Parameter	Value
Flap extent	$\eta = [0.7, 0.8]$ and $[0.7, 0.85]$
Flap chord	25% blade chord
Flap overhang	53% flap chord
Offset mass	18% sectional mass, 0.75% of total blade mass
Offset distance	21% blade chord
Flap frequency	0.014 Hz (9% of 1P)
Hinge preload	Tuned for null flap rotation at 9.5 m/s

4. Results

After the preliminary sizing of the passive flap presented in the previous section, two of the most interesting configurations are subjected to a more complete performance and load assessment analysis, as required by certification standards (IEC 61400-1, 2005).

4.1. Standard design conditions

The standard power production range was considered by DLC 1.1, from cut-in to cut-out wind speeds in 2 m/s increments, averaging over four different turbulent seeds (Jonkman and Buhl, 2006). AEP percent variations with respect to the baseline configuration are -0.5% and -0.55% for the normal and extended-span flaps, respectively. Both are non-negligible. To understand the effective impact of the AEP loss in terms of CoE, one would have to perform a more complete analysis than the present one. For example, one could design a rotor with a larger swept area

at similar key loads by exploiting the load alleviation provided by the passive flap. Such an analysis, although very useful for more fully characterizing the potential of the passive flap concept, is however considered as outside of the scope of the present work.

Figure 8 reports the flap angle mean and standard deviation in the relevant DLCs. Looking at the mean value, significant changes –especially for the smaller span flap– are encountered within the operating range, due to the hinge constant preload and in accordance with section 2. The standard deviation is an indicator of flap activity, which appears to be almost constant and similar for both span extensions between 4 to 19 m/s, and then tends to grow at the higher wind speeds.

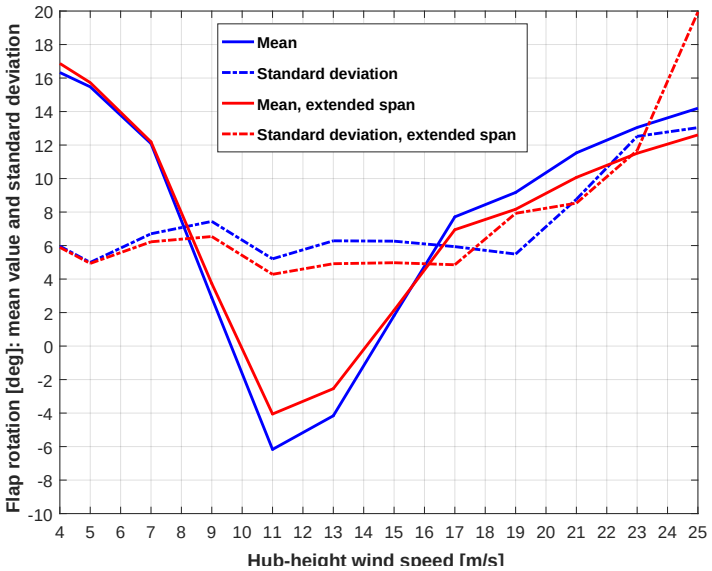

Figure 8: Flap angle vs wind speed in relevant DLCs. Mean value and standard deviation

DELs are evaluated at each verification station at a number of points on the perimeter of the section, and the point with the largest overall damage is selected. DELs of the combined moment at blade root, main bearing and tower base are reported in Fig. 9.

The passive flap appears to be lowering fatigue loads at the main bearing and tower base to a considerable degree. The increased authority of the solution with a larger spanwise extent is also clearly visible. The ample load reduction at tower base is due to the flap response to tower top accelerations caused by thrust fluctuations. At the main bearing, load reductions are driven by blade flapping. At the blade root, there is no appreciable DEL reduction in the combined moment, because the load attenuation in the flapwise direction is cancelled by the increase of the in-plane component. In fact, Fig. 10 reports the DELs of the flapwise, edgewise and torsional blade root components. The figure shows an increase in the edgewise loading due to the heavier weight of the flapped blade, but also due to the larger drag fluctuations caused by flap deflections. Looking at the flapwise component, an appreciable DEL reduction can be

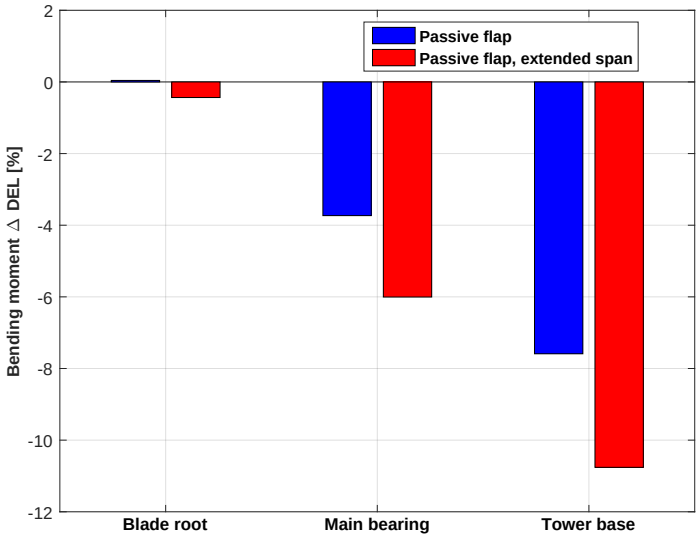

Figure 9: Weibull-weighted combined-moment DEL variations with respect to the baseline.

observed, which is responsible for the similar fatigue alleviation at the main bearing. The torsional moment records a significant increase, due to the increased pitching moment fluctuation generated by the passive flap deflection. Possibly, this load component might be reduced by the addition of a leading edge flap, as done for example in Lambie et al. (2011), however at the cost of an increased complexity of the system.

The collective pitch activity of the wind turbine is reported in Fig. 11. The plot shows the actuator duty cycle (ADC) as a function of hub-height wind speed, where the ADC is computed as

$$\mathrm{ADC} = \frac{1}{T}\int_0^T |\dot{\beta}|\,\mathrm{d}t, \tag{11}$$

where T is the duration of each turbulent simulation, and $\dot{\beta}$ the pitch rate of change. The reduction is noticeable and similar for both flap apertures. This effect can be attributed to the smoothing of the airloads performed by the passive device, which in turn yields a smoother response of the machine and a consequent reduced activity of the controller in reaction to wind fluctuations.

An ultimate load analysis was performed by considering a selected set of DLCs, chosen among the ones that drive the design of key components of the baseline wind turbine. DLC 1.1 and 1.3 consider power production in standard and extreme turbulence conditions. In DLC 2.3, a deterministic gust occurs in conjunction with a grid loss, and the effects of the fault time are examined by multiple simulations. Finally, DLC 6.2 considers parked conditions with a concurrent grid failure, where multiple yaw conditions are considered to identify the worst scenario.

Figure 12 reports the percent variations of the ultimate combined moments at blade root, main bearing and tower base. Better performance is achieved at the main bearing and at the blade root, where ultimate loads are generated in DLC 1.3 conditions. As in the case of fatigue damage, the passive flap seems to be able to smooth out airloads, with a

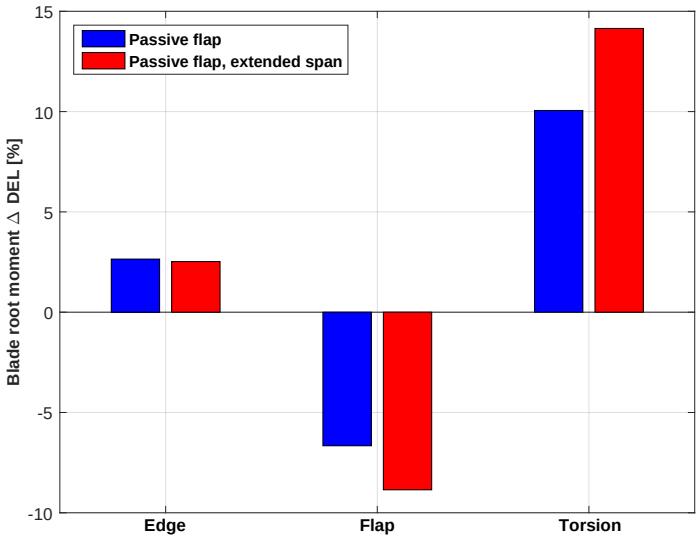

Figure 10: Flap, edge and torsional components of Weibull-weighted DEL variations with respect to the baseline.

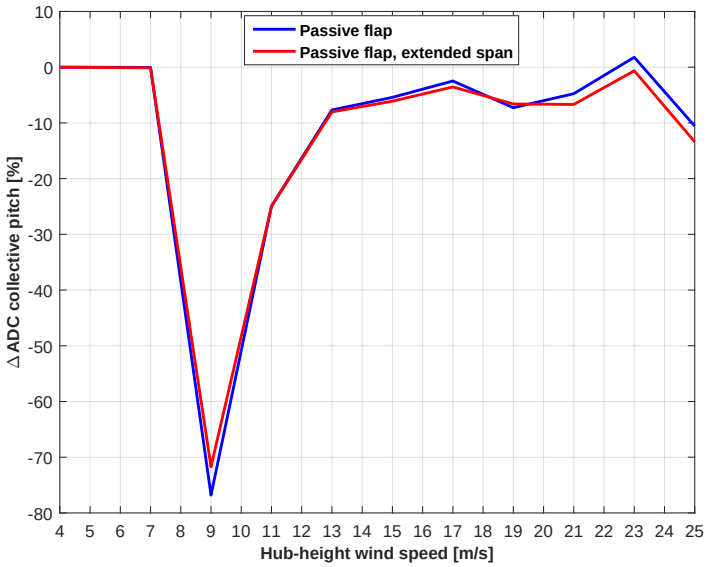

Figure 11: ADC variation percentage with respect to the baseline.

beneficial effects not only on fatigue but also on peak loads. As for the previous results, even in this case the extended flap span shows a greater authority.

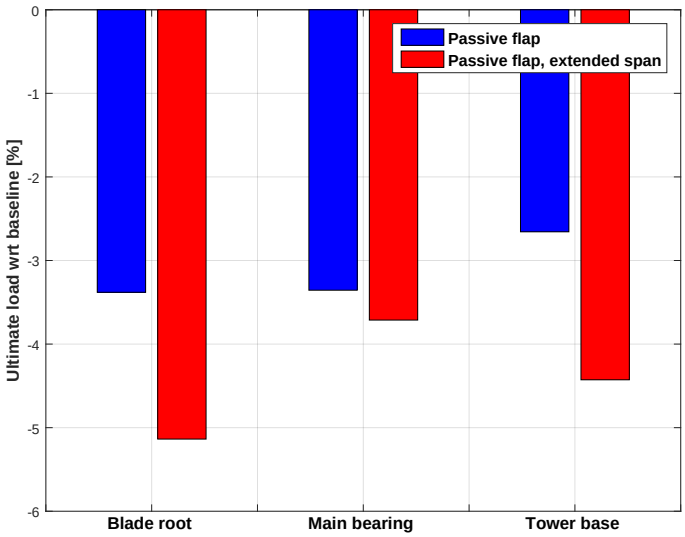

Figure 12: Percent variation of ultimate loads with respect to the baseline.

Ultimate tower base moments are generated in stormy DLC 6.2 conditions. In this case the observed load reductions are due to a reduced sail area of the blade, since the flap remains deflected in proximity of its stops.

4.2. Off-design conditions

Next, the effects of a failure of the passive flap system is considered. A fault scenario is defined by blocking the relative rotation of one of the flaps, creating an unbalanced behavior of one of the blades with respect to the other two. The wind turbine is supposed to be equipped with a safety system capable of detecting a failure and triggering an emergency shut-down procedure. Generator fault or loss of electrical grid are not included in the fault scenario, because two simultaneous malfunctions are considered to be unlikely.

Passive flap fault conditions are verified by DLC 2.1 and 2.3, with the scope of identifying the most demanding situation. For DLC 2.1 NTM simulations, a passive flap fault is imposed in conjunction with a large positive steep gradient or a maximum of the hub-height wind speed. DLC 2.3 simulates a deterministic extreme operating gust (EOG) at cut-out, rated and rated ± 2 m/s wind speed. In total, 16 simulations were performed at each wind speed, varying the time interval between the gust and the fault as well as the azimuthal position of the faulty blade.

The off-design performance is investigated by ranking in decreasing order the ultimate loads of the standard envelope plus the fault conditions, and looking at the maximum load peak. The first three ranking combined moments at tower base are reported for each configuration in Fig. 13, where fault conditions are identified by using light-gray-shaded bars. The ranking analysis for blades and main bearing are not reported here, because fault conditions do not

modify the highest three ranking loads. Results show that a passive flap fault does not dominate the load envelope, and therefore it is not a concern for the ultimate load state of the machine.

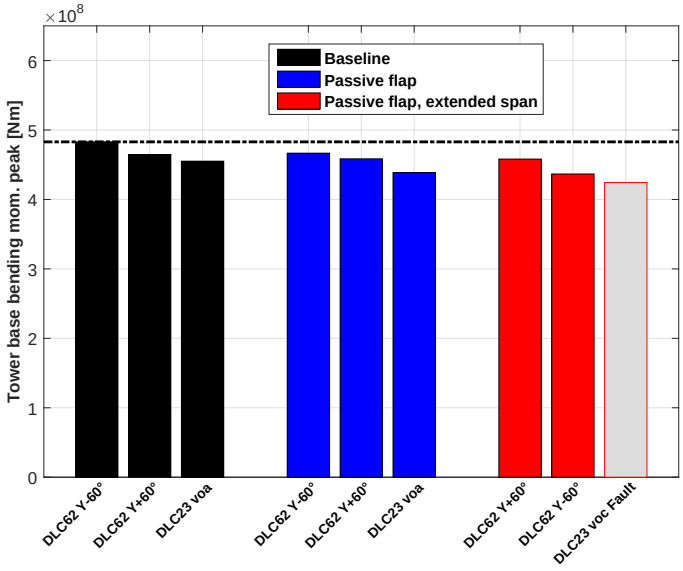

Figure 13: Ranking analysis of ultimate tower base combined moments. Passive flap fault conditions are displayed using light-gray-shaded bars.

5. Conclusions

A passive flap concept for load mitigation on wind turbines has been investigated in this paper by a detailed and geometrically exact multibody aeroservoelastic model. The study has considered the application of the passive flap to a very large conceptual 10 MW offshore wind turbine. The flap motion is driven by an offset mass, which, responding to blade accelerations, mitigates the dynamic loads on the machine. At first, the study has considered a general sizing of the device parameters. Next, a more complete assessment has been conducted of the overall machine performance and loading, considering fatigue and ultimate states. Following accepted standard certification procedures, the analysis has also considered the effects of one faulty stuck flap.

Based on the results of the present investigation, the following conclusions can be drawn:

- The proposed passive flap solution improves on the baseline in terms of both fatigue and ultimate loads.
- The more significant effects on fatigue are reported at tower base. This is due to tower top accelerations driving passive flap deflections, which result in a smoothing of the airloads. Fatigue at the main bearing is also reduced, and this is essentially due to passive device fluctuations driven by blade flapping. On the other hand, the overall fatigue at blade root is essentially unchanged. The analysis on the individual bending components reveals that,

while the flapwise alleviation is considerable, the weight of the flap offset mass increases edgewise bending fluctuations.

- Blade torsional fatigue is increased, due to the increased pitching moment fluctuation generated by the passive flap deflection. On the other hand, the overall actuator duty cycle of the pitch system is reduced. In fact, due to the smoothing of the airloads, the on-board control systems has to pitch less in response to wind turbulence with the passive flap than without it.
- Ultimate loads are considerably decreased at blade root, main bearing and tower base. Therefore the passive flap system positively affects both fatigue and ultimate loads.
- The consequences of device faults are limited, with no effects on ultimate design-driving loads.
- An increased flap spanwise extension improves the authority of the device, with consequent further load benefits, at the price of larger AEP losses.
- A simple solution using a constant preload guarantees interesting results in terms of load alleviation, with some AEP reduction. A more complex solution using a screw joint essentially eliminates energy yield losses, although it seems to be less effective in terms of load mitigation.

The results of this investigation are preliminary, and further studies are needed to fully understand the real possible capabilities and effectiveness of the passive flap concept. Nonetheless, the rather limited reduction in energy yield and noticeable mitigation of both ultimate and fatigue loads opens the door for a more in depth analysis of this concept. In particular, it would be interesting to exploit the reduction in loading to design a new rotor with a larger swept area and similar key loads of the baseline. This way one might more fully understand and quantify the effects of this solution on CoE.

Acknowledgements

Support of the FP7 INNWIND.EU project at the Politecnico di Milano is gratefully acknowledged.

References

ESDU, 1989. Item No. 89010, Example of Procedure in Calculation of Control Hinge Moments.

ESDU, 1989. Item No. AERO C.04.01.03, Effect of Nose Balance on Two Dimensional Control Hinge Moment Coefficients.

INNWIND.EU Design of State of the Art 10-20 MW Offshore Wind Turbines. http://www.innwind.eu/.

Wind Turbines — Part 1: Design Requirements, Ed. 3. International Standard IEC 61400-1, 2005.

Andersen, P. B., Henriksen, L., Gaunaa, M., Bak, C., Buhl, T., 2010. Deformable trailing edge flaps for modern megawatt wind turbine controllers using strain gauge sensors. Wind Energy, 13, 193–206, DOI: 10.1002/we.371.

Bergami, L., Poulsen, N. K., 2015. A smart rotor configuration with linear quadratic control of adaptive trailing edge flaps for active load alleviation. Wind Energy, 18, 625–641, DOI: 10.1002/we.1716.

Bernhammer, L.O., De Breuker, R., Van Kuik, G.A.M, 2016. Fatigue and extreme load reduction of wind turbine components using smart rotors. Journal of Wind Engineering & Industrial Aerodynamics, 156, 84–95, DOI: 10.1016/j.jweia.2016.04.001.

Chow, R., van Dam, C.P., 2007. Computational investigations of deploying load control microtabs on a wind turbine airfoil. 45th AIAA Aerospace Sciences Meeting and Exhibit, Reno, NV, USA, DOI: 10.2514/6.2007-1018.

Bak, C., Zahle, F.,Bitsche, R., Kim, T., Yde, A., Henriksen, L.C., Andersen, P.B., Natarajan, A., Hansen, M.H., 2013. Description of the DTU 10 MW Reference Wind Turbine. DTU Wind Energy Report-I-0092.

Bauchau, O.A., Rodriguez, J., Bottasso, C.L., 2001. Modeling of unilateral contact conditions with application to aerospace systems involving backlash, freeplay and friction. Mechanics Research Communications, 28, 571–599.

Bauchau, O.A., Bottasso, C.L., Nikishkov, Y.G., 2001. Modeling rotorcraft dynamics with finite element multibody procedures. Mathematics and Computer Modeling, 33, 1113–1137.

Bauchau, O.A., Bottasso, C.L., Trainelli, L., 2003. Robust integration schemes for flexible multibody systems. Computer Methods in Applied Mechanics and Engineering, 192, 395–420, DOI: 10.1016/S0045-7825(02)00519-4.

Bauchau, O.A., Epple, A., Bottasso, C.L., 2009. Scaling of constraints and augmented Lagrangian formulations in multibody dynamics simulations. Journal of Computational and Nonlinear Dynamics, 4(2), DOI: 10.1115/1.3079826.

Bortolotti, P., Bottasso, C.L., Croce. A., Sartori, L., 2017. Integration of multiple passive load mitigation technologies by automated design optimization — The case study of a medium-size onshore wind turbine. Wind Energy, under review.

Bottasso, C.L., 2010. Computational Dynamics. Encyclopedia of Aerospace Engineering, R. Blockley, W. Shyy, Eds., ISBN 978- 0-470-75440-5, John Wiley & Sons, Ltd.

Bottasso, C.L., Croce, A., 2006–2017. `Cp-Lambda` User's Manual. Dipartimento di Scienze e Tecnologie Aerospaziali, Politecnico di Milano, Milano, Italy.

Bottasso, C.L., Croce, A., Nam, Y., Riboldi, C.E.D., 2011. Power curve tracking in the presence of a tip speed constraint. Renewable Energy, 40, 1–12. DOI: 10.1016/j.renene.2011.07.045.

Bottasso, C.L., Croce, A., Devecchi, D., Riboldi, C.E.D, Nam, Y., 2013. Multi-layer control architecture for the reduction of deterministic and non-deterministic loads on wind turbines. Renewable Energy, 51, 159–169.

Bottasso, C.L., Croce, A., Gualdoni, F., Montinari, P., 2016. Load mitigation for wind turbines by a passive aeroelastic device. Journal of Wind Engineering and Industrial Aerodynamics, 148, 57–69. DOI: 10.1016/j.jweia.2015.11.001.

Bottasso, C.L., Croce. A., Gualdoni, F., Montinari, P., Riboldi, C.E.D., 2016. Articulated blade tip devices for load alleviation on wind turbines. Wind Energy Science, 1, 297–310. DOI: 10.5194/wes-1-297-2016.

Croce, A., Gualdoni, F., Montinari, P., Riboldi, C.E.D., Bottasso, C.L., 2016. Inertial and aerodynamic tuning of passive devices for load alleviation on wind turbines. Journal of Phisics: Conference Series, Vol. 753. DOI: 10.1088/1742-6596/753/10/102005.

Drela, M., Yougren, H., 2001. Xfoil Subsonic Air Development System, http://web.mit.edu/drela/Public/web/xfoil/xfoil_doc.txt.

Hansen, M.O.L., 2008. Aerodynamics of Wind Turbines, 2nd Edition. Earthscan.

Jonkman, B. J., Buhl, M.L., 2006. TurbSim User's Guide. Golden, Co, National Renewable Energy Laboratory.

Kelley, N., Jonkman, B., 2015. NWTC Computer-Aided Engineering Tools: TurbSim, http://wind.nrel.gov/designcodes/preprocessors/turbsim/.

Lambie, B., Jain, P., Tropea, C., 2011. Passive camber change for wind turbine load alleviation. AIAA Aerospace Sciences Meeting including the New Horizons Forum and Aerospace Exposition, Orlando, Florida, USA.

Marten, D., Spiegelberg, H., Pechlivanoglou, G., Nayeri, C. N., Paschereit, C. O., Tropea, C., 2015. Configuration and numerical investigation of the adaptive camber airfoil as passive load alleviation mechanism for wind turbines. 33rd AIAA Applied Aerodynamics Conference. DOI: 10.2514/6.2015-3390.

Peters, D. A., Cheng, J. H., 1995. Finite state induced flow models. Part II - Three-dimensional rotor disk. Journal of Aircraft, 32, No. 2(1995), 323–333. DOI: 10.2514/3.46719.

Stroub, R.H., 1982. An Analytical Investigation of the Free-Tip Rotor for Helicopters. NASA Technical Memorandum 81345.

Theodorsen, T., Garrik, I.E., 1942. Nonstationary Flow About a Wing-Aileron-Tab Combination Including Aerodynamic Balance. Tech. Report 736, NACA.

Wentz, W.H., Snyder, M.H., Calhoun, J.T., 1980. Feasibility study of aileron and spoiler control systems for large horizontal axis wind turbines, NASA Tech. Report, DOE/NASA/3277-1-NASA CR-159856 WER-10, http://ntrs.nasa.gov/archive/nasa/casi.ntrs.nasa.gov/19800019302.pdf